RESEARCH ARTICLE

Key Points:
- The Agulhas ring caused perturbations in the water properties structure down to 2000 m, with several distinct water source types
- The ring is a decaying Rankine vortex with its inner core in solid-body type rotation and its outer band in near-constant tangential speed
- The rings have a relatively minor contribution to the latitudinal heat and salt transport by the returning limb of the AMOC

Correspondence to:
A. Hernández-Guerra,
alonso.hernandez@ulpgc.es

Characteristics and evolution of an Agulhas ring

M. Casanova-Masjoan[1] (ID), J. L. Pelegrí[2] (ID), P. Sangrà[1], A. Martínez[1] (ID), D. Grisolía-Santos[1] (ID), M. D. Pérez-Hernández[3] (ID), and A. Hernández-Guerra[1] (ID)

[1]Instituto de Oceanografía y Cambio Global, IOCAG, Universidad de Las Palmas de Gran Canaria, ULPGC, Spain, [2]Departament d'Oceanografia Física i Tecnològica, Institut de Ciències del Mar, CSIC, Barcelona, Spain, [3]Department of Physical Oceanography, Woods Hole Oceanographic Institution, Woods Hole, Massachusetts, USA

Abstract A South Atlantic ring is studied through remote sensing altimetry, hydrographic stations, and drifters' trajectories. The ring's core was characterized by warmer and saltier Indian Ocean waters. At the time of the cruise, the ring's signature extended radially out to 124 km and vertically down to 2000 m, and its core absolute dynamic topography (ADT) exceeded the surrounding Atlantic Ocean waters in 0.4 m. The geostrophic velocities were anticyclonic with maximum speeds about 35 cm s^{-1} at 100 m and reaching negligible values near 4500 m. The rotational transport inside the ring was 33 Sv in the thermocline and intermediate layers. The drifters' data distinguish a 30-km core revolving as a solid body with periodicity near 5 days and a transitional band that revolves with constant tangential velocity, resembling a Rankine vortex. The ADT data identify the ring's track, showing that it was shed by the Agulhas Current retroflection in November 2009 and propagated northwest rapidly during the first 2 months (mean speed of about 10 cm s^{-1}) but slowed down substantially (3–4 cm s^{-1}) between March and July 2010, when it was last detected. The altimetry data also outlines the evolution of the ring's core ADT, radius, vorticity, and, through a simple calibration with the cruise data, rotational transport. In particular, the ring surface and vertical-mean vorticity decay with time scales of 373 and 230 days, respectively, indicating that most of the property anomalies contained by the ring are diffused out to the subtropical gyre before it reaches the western boundary current system.

1. Introduction

South of Africa, the westward Agulhas Current (AC) encounters the eastward South Atlantic (SAC) and Antarctic Circumpolar (ACC) Currents. The outcome is the AC retroflection (ACR) (15–20°E) as a tight loop that is regularly occluded and sheds warm and salty anticyclonic rings with the same physical and chemical characteristics as the AC: their surface core is warmer (up to about 5°C) and saltier (up to 1 unit) than the surrounding South Atlantic surface waters [*Biastoch and Krauss*, 1999; *Garzoli et al.*, 1999; *Gordon and Haxby*, 1990; *Gordon et al.*, 1992; *Lutjeharms*, 2007]. The young ACR rings are among the largest and most energetic eddies of the world [*Richardson*, 2007; *Lutjeharms*, 2007], releasing about 50% of its potential energy within 600 km from formation [*Arhan et al.*, 1999]. Small cyclones are also formed in the ACR, typically remaining close to the retroflection before being transported south to the SAC-AAC system and returning to the Indian Ocean [*Biastoch and Krauss*, 1999; *Garzoli et al.*, 1999; *Gordon and Haxby*, 1990; *Richardson*, 2007].

The anticyclonic ACR (ac-ACR) rings follow north and northwest as vortices transported by the South Equatorial and Benguela Currents in a beta plane—a positive combination of mean-flow advection and self-induced motion [*Biastoch et al.*, 2008; *Gordon and Haxby*, 1990; *Lutjeharms*, 2007; *McDonagh et al.*, 1999; *Richardson et al.*, 2003]. The ac-ACR rings are substantially large (mean diameter of 200–400 km) and have typical mean depths of 1500–2000 m [*Biastoch and Krauss*, 1999; *McDonagh et al.*, 1999], although *van Aken et al.* [2003] found a ring that reached down to 4500 m. These properties change with the shedding season and the time they remain in the retroflection area [*Lutjeharms*, 2007]. After formation, the sea-surface absolute dynamic topography (ADT) in the core of the rings may typically exceed 1 m above the outer mean levels, driving rotational near-geostrophic velocities in excess of 1 m s^{-1}. These high speeds and the large diameter of the rings cause large rotational geostrophic transports, some 20–30 Sv [*Gordon and Haxby*, 19990].

About nine ac-ACR rings spin off from the AC every year, with some five or six crossing the Atlantic Ocean along the rim between the subtropical and tropical gyres (the Agulhas Ring Corridor) with lifetimes of 2–4 years [*Biastoch and Krauss*, 1999; *Garzoli et al.*, 1999; *Gordon and Haxby*, 1990; *Richardson*, 2007; *Schouten*

et al., 2000]. One interpretation of these relatively long lifetimes is that a ring transfers a small fraction of its thermodynamic content to the Atlantic Ocean, in agreement with recent observations by *Wang et al.* [2015], apparently because of coherent structures surrounding the ring that may prevent such exchange [*Wang et al.*, 2016]. The mean ring propagation rate, as estimated from floats and GEOSAT altimetry track data, ranges between 4.4 and 8.3 cm s^{-1} [*Gordon and Haxby*, 1990; *Richardson*, 2007]. These propagation values, together with their relatively long lifetimes, imply that most rings reach the western boundary region after a transatlantic journey of 2–3 years [*Gordon and Haxby*, 1990].

The rings account for approximately 15 Sv [*Garzoli et al.*, 1999; *Richardson*, 2007] and 0.3–0.4 PW [*Souza et al.*, 2011], hence potentially compensating for most of the water mass (17–18 Sv) and net heat (0.35 and 0.77 PW at 35 and 19°S, respectively) transport by the Atlantic Meridional Overturning Circulation (AMOC) [*Rahmstorf and England*, 1997; *Toggweiler and Samuels*, 1995; *Ganachaud and Wunsch*, 2000, 2003; *Mercier et al.*, 2015]; the difference between the water mass transport by these rings and the AMOC actually lies within the observational uncertainties [*Hernández-Guerra et al.*, 2014].

Considering their long lifetimes and large transport, it may appear as if the warm Agulhas rings could have a substantial contribution to the northward transport of water mass and heat in the South Atlantic. However, when these long-lived rings reach the western boundary system they follow south with the Brazil Current [*Lutjeharms*, 2007]. Accordingly, rings will contribute to the AMOC only after decaying within the subtropical gyre, what would guarantee that a large fraction of their input to the subtropical gyre gets transferred to the tropical gyre, mainly through the North Brazil Current (NBC) [*Lazar et al.*, 2002; *Rodrigues et al.*, 2007], something not to be expected according to *Wang et al.* [2015, 2016].

Here we will investigate the rate of decay of these rings—or rate of transfer of key properties such as heat, salt and vorticity—to the interior South Atlantic Ocean during their westward trip. Our analysis combines satellite, hydrographic, and drifter data to characterize an Agulhas ring surveyed in early March 2010, as well as to provide some insight onto the temporal evolution of the ring's properties from its formation, 5 months earlier and 1000 km away, till its merging with other mesoscale structures, in late July 2010.

The conductivity-temperature-depth (CTD) stations crossed the ring through its center down to the seafloor, providing a good description of its vertical structure and water masses. They also allow determining the vertical structure of geostrophic velocities for pure rotational vertically integrated transport, a set of velocities that is consistent with the surface velocities as inferred from both altimetry and drifter data. The drifter data, lasting some 50 days inside the ring, is also used to calculate the speed of the ring core and to examine the radial structure of the orbital velocities. The altimetry data further provides the ring's trajectory and surface characteristics since its formation, vorticity among them.

Knowing the surface vorticity and total ring's rotational transport at the time of the cruise, and assuming a simple relation between surface vorticity and transport, we can estimate the temporal evolution of the rotational transport for the entire ring's lifetime. These variables lead to an exponential-decay time scale of the ring's vorticity that turns out to be comparable with the time scales for heat and salt transfer, as simply deduced from the temperature and salinity at origin (AC) and during the cruise. These scales may be used to provide meaningful insights on the rate of cumulative transfer of properties from the ACR rings to the entire South Atlantic subtropical gyre.

The paper is organized as follows. Section 2 introduces the data set and methods used to characterize the Agulhas ring and its evolution. Section 3 presents the vertical structure of properties and water masses (section 3.1), the surface evolution of the ring from altimetry (section 3.2), the trajectories of the drifters while inside the ring (section 3.3), and the vertical structure of the velocity fields as inferred from the CTD data (section 3.4). Section 4 explores the temporal evolution of the ring properties, including the radial distribution of velocity and vorticity, and provides estimates for the rate of vorticity transfer to the surrounding waters. We close with a discussion of the main results and some concluding remarks in section 5.

2. Data and Methods

2.1. Hydrography
The CTD data were collected during the oceanographic cruise MOC2-Austral onboard the R/V Hespérides, from 8 February to 10 March 2010, between Ushuaia and Cape Town in the South Atlantic. For this study,
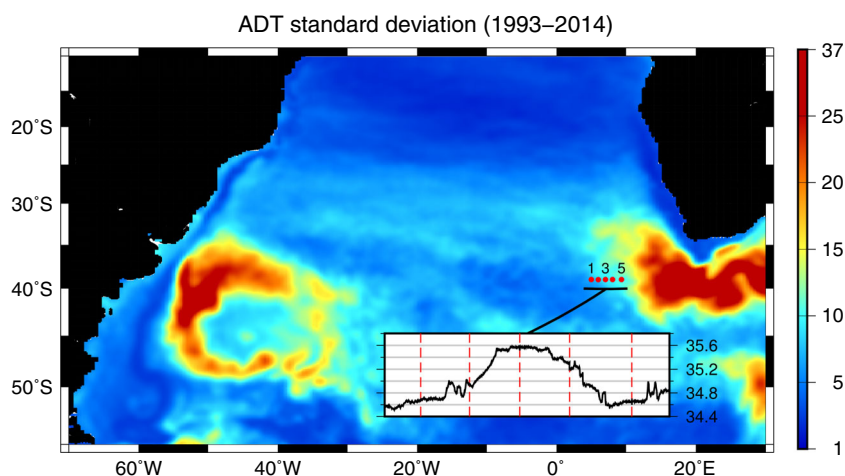
Figure 1. Map of the South Atlantic ADT standard deviation with the location of hydrographic stations (red circles) and corresponding sea surface salinity as observed with the vessel's termosalinograph (inset). The color bar displays the standard deviations (cm), with colors saturated at 25 cm though maximum values reached 37 cm. The red-dashed lines in the inner plot indicate the location of the hydrographic stations.

we have selected data from five hydrographic stations done on 4–5 March, hereafter numbered as stations 1 through 5 (from west to east). Figure 1 depicts the location of the hydrographic stations, the near surface salinity values as obtained from the onboard termosalinograph during the zonal track, and the ADT standard deviation distribution as calculated using the Archiving, Validation, and Interpretation of a Satellite Oceanographic (AVISO) database (downloaded from http://www.aviso.altimetry.fr/) [*AVISO*, 2015]. The surface salinity shows a high-salinity core with rather constant values of 35.6, which is the signal of the Agulhas Ring; station 3 was within the core, stations 2 and 4 sampled its outer ring and stations 1 and 5 have the surface salinity values of the environment surface Atlantic Water. The altimetry data confirms that the ring was located in the Agulhas ring corridor, as also shown by *van Sebille et al*. [2012] and *Mason et al*. [2017].

The thermal wind equations are used to obtain the geostrophic flow within the ring and the integrated transport. The neutral density surface of $\gamma_n = 28.2$ kg m^{-3}, at about 4500 m depth, is chosen as the level of no motion. This reference level provides surface geostrophic velocities that fit well the values as inferred from altimetry. Further, it ensures that the net latitudinal transport, after integration across the ring (from stations 1 to 5) and down to the reference depth, is very close to zero, i.e., the entire transport is rotational. We adopt the same neutral density levels as in *Ganachaud* [2003] in order to divide the mass transport in different layers.

2.2. Altimetry

Daily ADT values are obtained from the AVISO database for the region from 3 to 24°E and from 32 to 42°S, originally with a 1/4° resolution and later interpolated onto a 1/20° grid; the data encompasses nearly 10 months, from 4 October 2009 (formation date of the ring) to 25 July 2010 (when the ring fused with other mesoscale features and could not be further tracked with altimetry) (Figure 2). The altimetry maps depict the hydrographic stations cutting the Agulhas ring zonally through its central axis.

The altimetry maps also provide the times when the ring was shed and disappeared as well as the temporal evolution of its peak core ADT and radius. The ring trajectory is estimated as the grid point with maximum ADT daily values within the ring core. The ring radius is calculated as the mean distance between the maximum ADT and the contour of 0.5 m, which is considered to be the edge of the ring.

A time series for the ring's rotational transport is obtained from the daily radius and mean surface geostrophic rotational velocities, calibrated with the transports observed during the cruise. Specifically, the geostrophic velocities are calculated from the hydrographic data using a no-motion reference level of 4500 m. The mean rotational transport on 4–5 March is then calculated as a discrete summation of these geostrophic velocities, across the ring (either between stations 1 and 3 or between stations 3 and 5) and from the sea surface down to 4500 m. This value is then adjusted to the vertical integral of a mean rotational velocity v(z) times the radius, with the velocity decaying exponentially with depth, v(z)=v$_0$exp(−z/h), where h is a constant and v$_0$ is the mean surface velocity. The surface velocity v$_0$ is inferred from the ADT
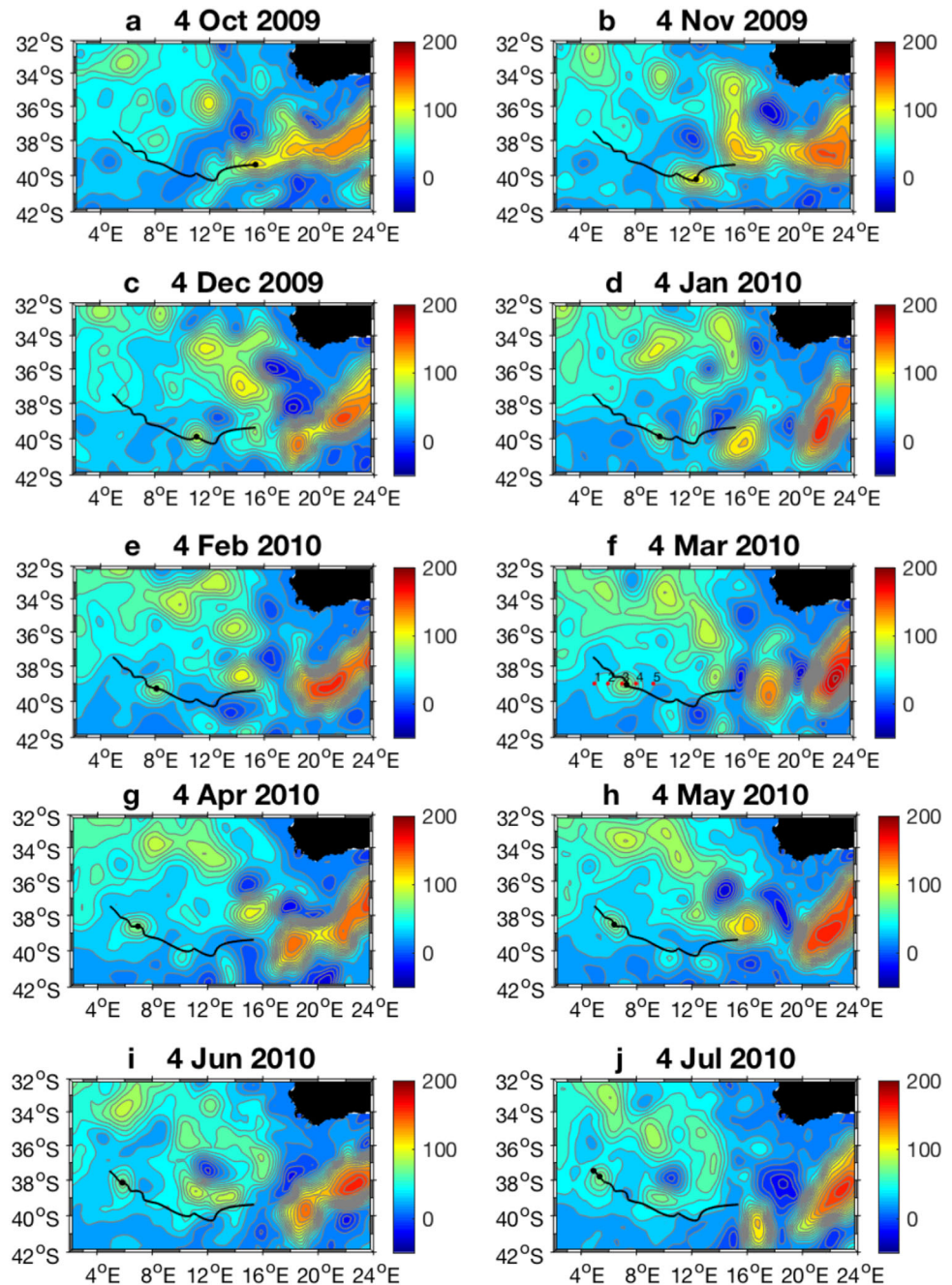
Figure 2. Daily ADT images (cm) southwest of South Africa, once a month between 4 October 2009 (first observation of the ring) and 4 July 2010 (day 274, 21 days before losing its ADT track). The track of the ring is shown as a black line, with the black dot positioning the ring on the date of the plot. The red dots in plot f show the hydrographic stations during the survey on 4–5 March 2010. The two dots in plot j indicate the location of the ring on 4 July (day 274) and the final location (day 295), just before the track of the ring was lost.

difference and lateral distance between the ring's core and the 0.5 m contour, and h is obtained as the value that provides the best fit to the observed transport, turning out to be h = 800 m. Once this function is known, and under the assumption that it remains constant over the ring's life, we estimate the temporal evolution of the rotational transport.

2.3. Drifters

Our study also includes positioning data every 6 h from two satellite-tracked near-surface drifters drogued at 15 m and deployed near stations 3 and 4. These are drifters 89771 and 89772 of the National Oceanic

and Atmospheric Administration (NOAA) Global Drifter Program (GDP), hereafter identified as D1 and D2, respectively. The quality control procedure of NOAA-GDP indicates that D1 and D2 lost their drogues only 32 and 4 days after deployment, respectively; despite this apparent early loss, we analyze the positioning data as explained next.

The drifters' data between early March and late April, while they remained within the ring, allow determining the ring's mean motion and rotational characteristics. The trajectory, mean radius, and revolution period of the ring are estimated following the methodology described in *Brassington* [2010]. This method assumes that drifters within ocean eddies follow Lagrangian trajectories that orbit a local geopotential extremum. The first step is to remove the inertial motions (inertial period is about 19 h) by applying a 36 h low-pass Butterworth filter to the positioning data. Under the assumption that the drifter's trajectory inside an eddy oscillates, the method locates the extreme zonal and latitudinal positions and interpolates the positions with a cubic spline, positioning the ring's center and the drifter's orbit (rotational period and radius). The method provides a smooth change in the radius but leads to somewhat rapid and small fluctuations in the periods, which are then averaged to provide an equally smooth (but somewhat shorter) time series.

The above method simultaneously provides the radial position and orbital velocities of the drifters. These are then used to produce scattered plots of vorticity and tangential velocity as a function of radial position, which is informative on the radial structure of the ring. Finally, a rotary wavelet analysis of the drifter-inferred velocity components lends the sign and rate of the drifter's rotation [*Sangrà et al.*, 2005; *Torrence and Compo*, 1998].

3. Results

3.1. Ring Hydrography

Vertical sections of potential temperature, salinity, neutral density, nitrates, alkalinity, and pH from the sea surface down to 2000 m are used to identify the ring's water masses (Figure 3). The v-shaped structure of all property contours reveals the presence of an anticyclonic eddy, with core waters of Indian Ocean origin at the surface and subsurface layers, identified as Agulhas Water (AGW).

The AGW is substantially warmer and saltier than the surrounding waters, with potential temperature and salinity as high as 16°C and 35.6 at 100 m, respectively (Figures 3a and 3b). This contrasts with the colder and fresher waters found in the outer stations, where the potential temperature and salinity at 100 m are below 12°C and 34.8, respectively. The temperature and salinity of these outer waters reflect their location between the subtropical and subantarctic fronts, what has been named the Subantarctic Zone [*Tsuchiya et al.*, 1994], hence corresponding to a region of formation of Subantarctic Mode Waters (SAMW) [*Tsuchiya et al.*, 1994; *Orsi et al.*, 1995]; this is also illustrated by the homogeneous salinity in the upper 200 m, indicative of the winter creation of this water type. This zonation is confirmed by the mean surface ADT values of the environment waters at these latitudes, of about 0.25–0.40 m (see next section), or in the range of values ascribed to lie just north of the northern subantarctic front [*Barré et al.*, 2011].

All water properties show substantial variations between the surrounding waters and the ring, as represented by its core characteristics: the nitrate concentration decreases from 7.3 μmol kg^{-1} outside the ring to 1.86 μmol kg^{-1} near its core [*van Aken et al.*, 2003] (Figure 3d); alkalinity increases from 2294 to 2332 μmol kg^{-1}, highly correlated with salinity (Figure 3e); pH has a trend similar to potential temperature, increasing from 7.85 to 7.96 [*González-Dávila et al.*, 2011] (Figure 3f).

A potential temperature versus salinity (θ-S) diagram clarifies what the ring represents in terms of intruding Indian Ocean waters into the eastern South Atlantic Ocean (Figure 4). The most remarkable signal appears in layers lighter than $\gamma_n = 26.8$ kg m^{-3}, corresponding to depths less than about 200 m outside the ring and some 600 m in the ring core, displaying AGW substantially saltier and warmer than the SAMW. In contrast, the Antarctic Intermediate Waters (AAIW, density range 26.8–27.75 kg m^{-3}, extending from 200/600 m outside/inside the ring down to about 1400 m) do not show significant differences between those stations located outside and inside the ring. This reveals that AAIW in the Atlantic and western Indian Oceans have similar θ-S structure [*Gordon et al.*, 1992; *Orsi et al.*, 1995]. In the lower part of this density range, there are differences that respond to the influence of Upper Circumpolar Deep Waters (UCDW) in the South Atlantic at densities of 27.4–27.75 kg m^{-3}, contrasting with some traces of Red Sea Water (RSW) brought about by
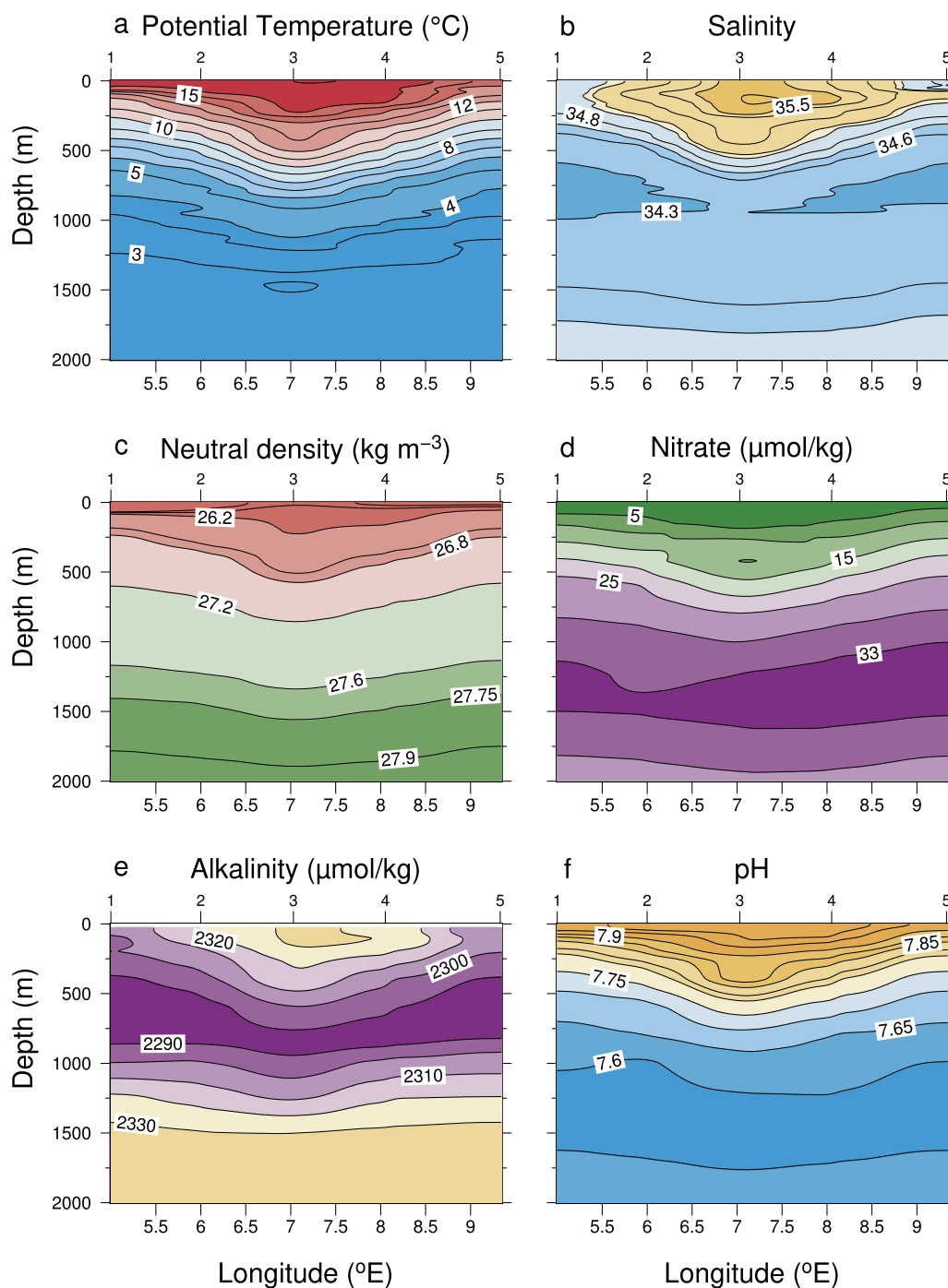
Figure 3. Vertical sections of (a) potential temperature (°C), (b) salinity, (c) neutral density (kg m^{-3}), (d) nitrates (μmol kg^{-1}), (e) alkalinity (μmol kg^{-1}), and (f) pH. The location of the stations is shown in the upper horizontal axis.

the AC in the density range 27.2–27.6 kg m^{-3} [*van Aken et al.*, 2003]. RSW penetrates into the AC from the South Indian Ocean, becoming a distinctive component of the intermediate waters at the ACR [*Lutjeharms and Ansorge*, 2001]. Below the intermediate waters, the ring θ-S anomalies disappear.

3.2. Ring Evolution From Altimetry

The daily AVISO altimetry maps are used to produce a monthly sequence of sea surface ADT, from October 2009 till July 2010 (Figure 2). The ring's date and place of formation is set to early October 2009 at (39°S, 15°E) (Figure 2a). Hereafter, we will take day 1 to start on 4 October 2009 at 0000 UTC, when the ring was
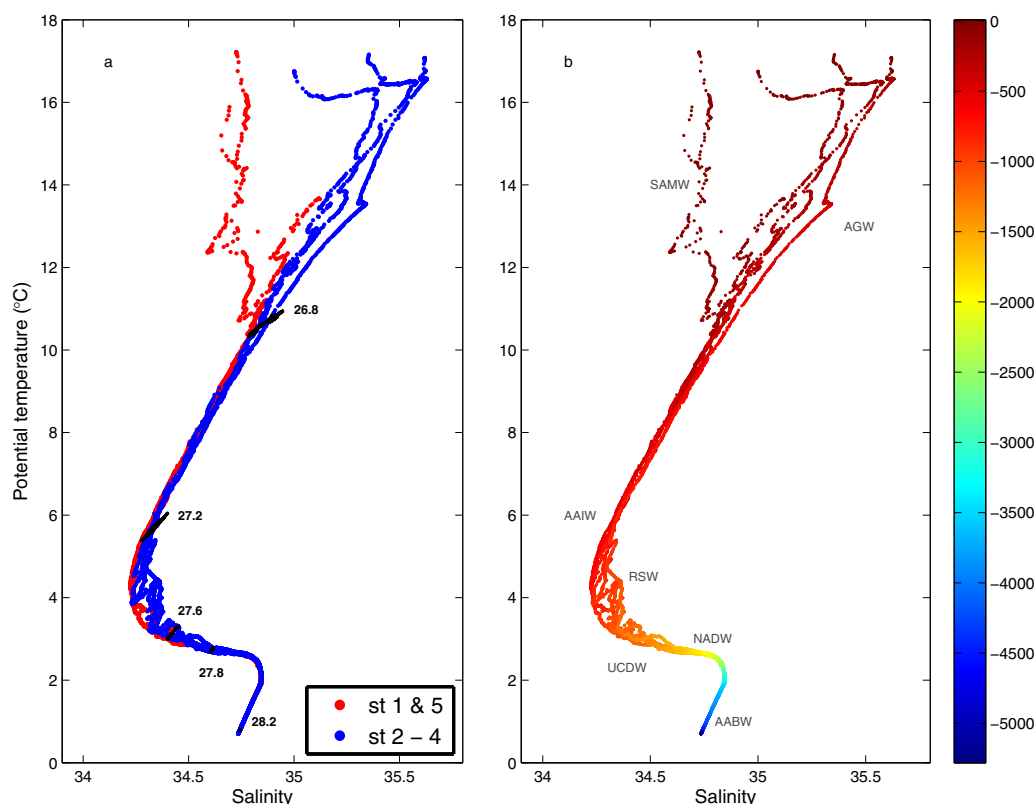
Figure 4. θ/S diagram using the data from the hydrographic stations across the Agulhas ring. (a) The red dots represent the data points from stations 1 and 5, and the blue dots represent the data from stations 2, 3, and 4; the black thick lines draw several selected neutral density values. (b) The data from all stations are color-colored with depth. The water masses are the following: Subantarctic Mode Water (SAMW), Agulhas Water (AGW), South Atlantic Central Water (SACW), Red Sea Water (RSW), Antarctic Intermediate Water (AAIW), Upper Circumpolar Deep Water (UCDW), North Atlantic Deep Water (NADW), and Antarctic Bottom Water (AABW).

shed by the Agulhas retroflection, with an ADT of 115 cm at its center. During its first 4 months (early October 2009 to late January 2010) the ring moved from the region of retroflection to the location of the hydrographic stations (red dots on the maps) (Figures 2a–2d). The ring reached (39°S, 8°E) in early February 2010 (Figure 2e). From 1 February to the time of the cruise sampling on 4 March 2010 (days 120–152), the ring moved only slightly, with its center remaining very close to station 3 and the core ADT nearly constant at 0.83 m (Figure 2f). From early March to the end of the surface track on 25 July 2010 (days 152–295), the ring continued slowly northwest, eventually reaching about (37.5°S, 5.0°E) while its core ADT decreased to 0.68 m (Figures 2g–2j). After 25 July 2010 (day 295), the ring could not be tracked with altimetry because it merged with other mesoscale features.

We may use the ADT at any time, in particular at the time of the hydrographic stations, to obtain the surface geostrophic velocity fields. Figure 5 shows the ADT field together with the corresponding sea-surface geostrophic velocity over the ring on 4 March 2010. This image illustrates the zonal track of the cruise through the ring, with station 3 near the ring's core. The ADT-inferred latitudinal velocity along the cruise track generally lies in the range of 0.2–0.3 m s^{-1} though the highest values approach 0.4 m s^{-1}, located away from the ring's core and near the 0.5–0.6 m ADT contours.

3.3. Drifter Trajectories

Drifters D1 and D2 were deployed near hydrographic stations 3 and 4, respectively, at the core and edge of the ring (Figures 1 and 5). The initial positions transmitted by D1 and D2 may be used to calculate the velocities of the drifters on 4–5 March, at the time of the hydrographic stations. A comparison of the low-passed drifter-inferred velocities with those values obtained from altimetry shows good agreement (Figure 5).

For our calculations, we consider a drifter to remain within the ring until 1 week previous to exiting the 0.5 m ADT contour. This 7 day stretch is chosen to avoid cotamination from the time series when the
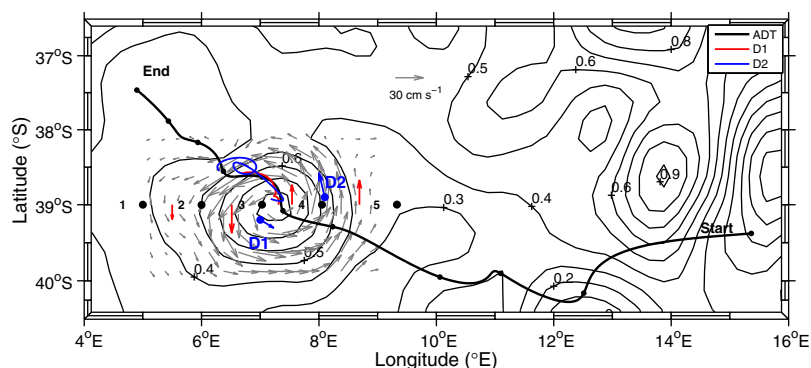
Figure 5. ADT on 4 March 2010 (contours every 0.1 m), with the 0.8 m isoline running over station 3. The black dots show the position of the hydrographic stations and the blue dots indicate where D1 and D2 were deployed. The bold black line is the ring's core trajectory from 4 October 2009 to 25 July 2010 as inferred from the altimetry data (with a tick mark every 30 days except the last interval that corresponds to 25 days), and the red and blue lines represent the ring's core trajectories from early March to late April as respectively inferred from D1 and D2. The gray arrows show the surface geostrophic velocity vectors as calculated from the ADT values, the blue arrows denote the drifters' velocities shortly after deployment and the red arrows are the geostrophic velocities as obtained from the hydrographic data; the reference velocity vector corresponds to 0.3 m s^{-1}.

drifter is already swiftly propagating away from the ring. Using this criterion, D1 and D2 remained within the ring during about 46 and 50 days, respectively, providing 39 and 43 days of data to characterize the ring. The original and low-passed (36-h Butterworth filter) drifters' trajectories, together with the corresponding ring center displacements, are illustrated in Figure 6.

While remaining inside the ring, both drifters had mean northwestward trajectories, 4.3 cm s^{-1} for D1 and 7.4 cm s^{-1} for D2; the northward velocity component is 1.9 and 1.1 cm s^{-1} for D1 and D2, respectively.

The ring orbits are obtained subtracting the displacement of the ring center to the drifters' trajectories (Figures 7a and 7b). These orbital motions then lead to the orbital velocities, radial positions, and corresponding rotational periods [*Brassington*, 2010]. Orbits for D1 were circular except for the last two revolutions, when
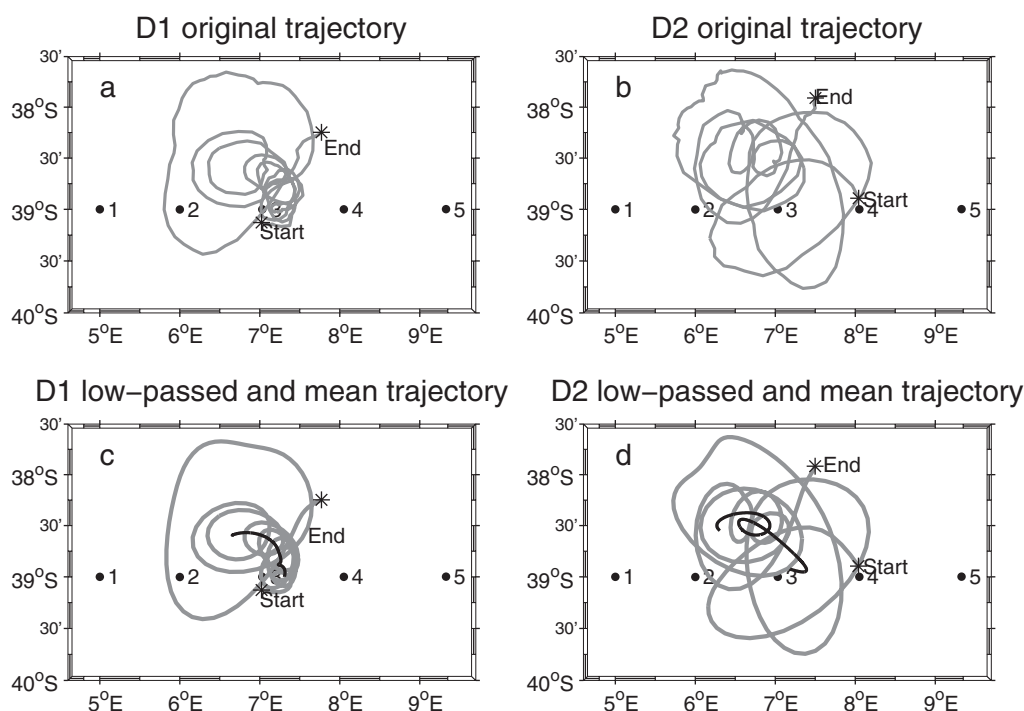
Figure 6. Row trajectories for (a) D1 and (b) D2. Low-passed (36 h Butterworth filter, *gray* line) and corresponding core trajectories (*black* lines) for (c) D1 and (d) D2. The black dots denote the position of the hydrographic stations.
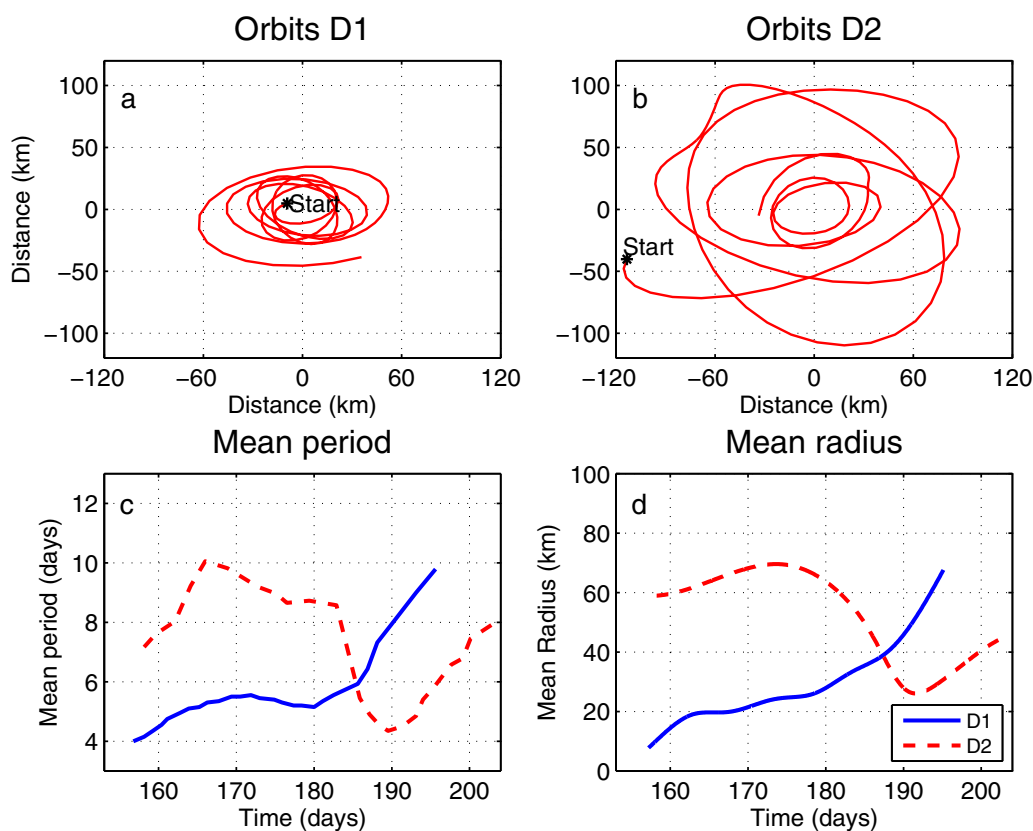
Figure 7. Orbits of (a) D1 and (b) D2. Time series of the mean rotational (c) period (days) and (d) radius (km) for drifters D1 (solid line) and D2 (dashed line).

they became elliptical with its major axis oriented zonally. As D1 was deployed closer than D2 to the center of the ring, it initially presented smaller amplitude and radius, about 5 days and 20 km, respectively; after some 25 days, the period increased progressively, up to 9 days, and the radius reached 50 km. In contrast, the orbits for D2 were initially elliptical, with its major axis oriented meridionally, with period and radius about 8–9 days and 60–70 km. D2 also approached the ring's core after some 25 days, or nearly three full orbits, and its period and radius decreased to 5–6 days and 30–40 km, respectively, remaining in this outer coordinate for another two revolutions. Both drifters exited the ring rather suddenly and moved east for several weeks before being trapped by another anticyclonic structure, strongly suggesting that neither drifter had completely lost their drogue. After eventually departing from this second mesoscalar feature, both drifters followed north, in what would be the predominant path of the Benguela Current.

A rotary wavelet spectral analysis of the orbital velocities helps assess the stability of the ring. Until about day 205, both drifters had little energy in the clockwise (CW) spectra as compared with the counterclockwise (CCW) spectra (Figure 8). The sharpness of the peak energy may be used to assess the stability of the ring at the radial position where the drifter is located. D1 displayed a sharp peak at 5 days, a situation that lasted some 25 days (days 157–182 in the time series). Afterward, the peak rapidly widened and, by day 192, became centered at a period of about 10 days. After day 205, the peak energy level decreased and shortly afterward it split in several bands. D2 also initially presented a relatively sharp energy peak (8–9 days) that lasted until about day 172. At this time, the energy spectrum split into two adjacent peaks, with the most intense one centered at 10 days. Between days 180 and 190, the short-period peak progressively intensified while the long-period peak vanished. Between days 195 and 205 one single peak reappeared, weaker and centered at periods of 7–8 days.

The time when the CCW peak energy begins to disperse, about day 205, coincides with the moment the CW energy displays a substantial increase (Figure 8). This leads us to appraise that both drifters left the ring at about the same time, roughly on day 205, after remaining inside the ring for a total of about 50 days. For
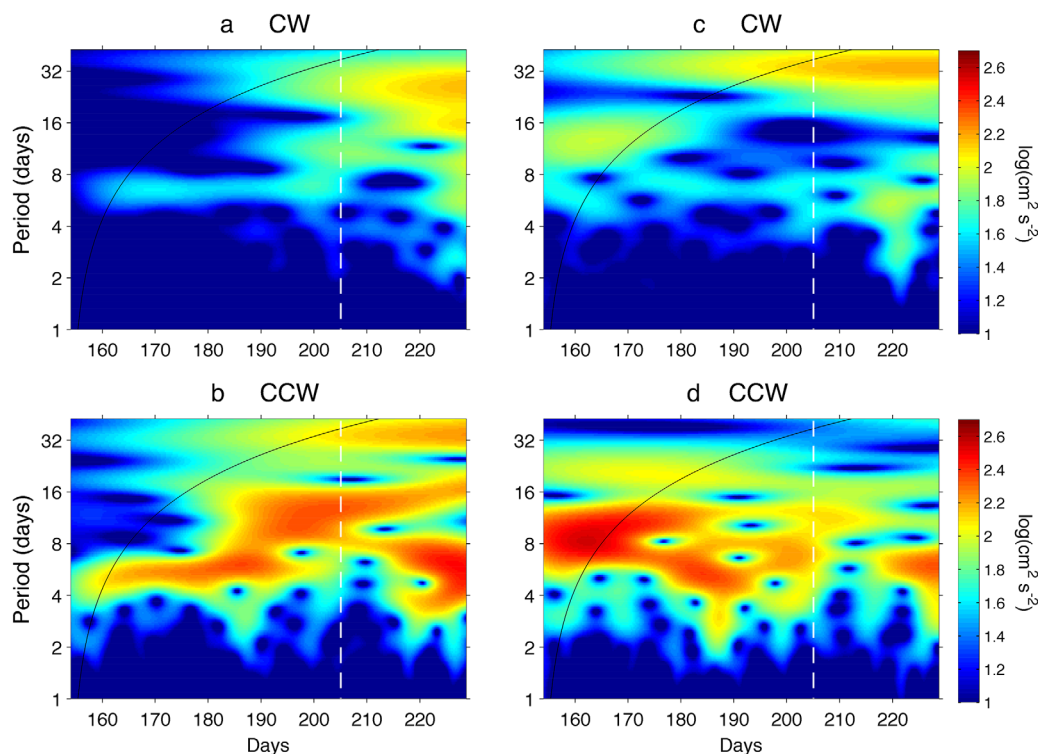
Figure 8. Rotary wavelet power spectrum for (a,b) D1 and (c,d) D2. Panels (a) and (b) show the clockwise (CW) and counterclockwise (CCW) components for D1, respectively; similarly with panels (c) and (d) but for D2. The black line is the cone of influence, where edge effects become important, and the white-dashed line indicates when the drifters exited the ring.

D2, this time lapse is exactly the same as inferred from the orbital motions, while it is slightly longer for D1 (from the orbital motions it was inferred to be 46 days).

The suspicion that both drifters lost their drogue early after deployment (32 and 5 days for D1 and D2, respectively) deserves further discussion. One first consideration is that the swift outward radial motion of D1 occurred only 25 days after deployment, and D2 remained at near-constant radial positions for a similar time lapse. Further, during the entire time the drifters remained inside the ring, the mean winds were of 8.5 m s^{-1} toward the southeast; in the absence of a drogue, a simple 3% wind-drift coefficient says that the wind-driven induced current would have been about 25 cm s^{-1}, much in excess of both the drifter mean and rotational speeds, i.e., without their drogue the drifters would have remained only a few days inside the ring. After exiting the ring, the drifters moved first to the northeast and later to the north (not shown), the natural path of the Benguela Current, rather than following the direction of the mean winds toward the southeast. About 3 weeks after leaving the ring, both drifters became trapped again by another anticyclonic feature: one drifter remained inside this structure 16 days and the other 19 days, or about three full revolutions; during this time the mean speed of both drifters was less than a few cm/s, something very unlikely unless the drifter had not loss its drogue. *Lumpkin et al.* [2013] have suggested that early (inaccurate) detection of the drogue loss is caused by incorrect performance of the submergence buoy values, requiring manual analysis of the positioning data; this is precisely what we have carried out, concluding that very likely both drifters had their drogue while revolving the Agulhas ring.

3.4. Geostrophic Velocity and Transport
The five CTD stations allow calculating four profiles of meridional velocity as a function of depth (Figure 9). Stations 1–3 (3–5) have southward (northward) flow, indicative of the ring's counterclockwise rotation. A no-motion reference level is chosen at 4500 m since, as explained in section 2.2, this level provides for a near-zero net latitudinal flow associated to the ring, i.e., the entire flow is rotational. This reference value also leads to surface velocities in good agreement with the values inferred from either the ADT fields or the drifters.
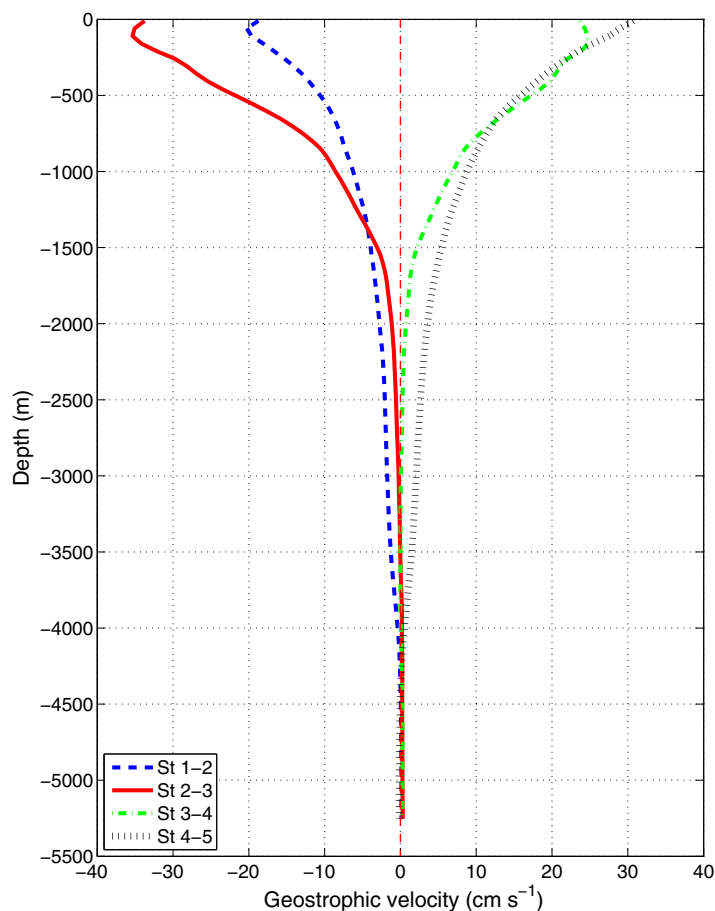
Figure 9. Geostrophic velocity as a function of depth, calculated from each pair of CTD stations with 4500 m as the zero-velocity reference level: 1–2 (dashed line), 2–3 (solid line), 3–4 (dash-dotted line), and 4–5 (dotted line).

The rotational velocity reaches maximum values at about 100 m depth, with a peak value in excess of 35 cm s^{-1} associated to the station pair 2–3; these sub-surface maxima speeds are caused by the salinity maximum at about 100 m and the associated change in the slope of the isoneutrals in the top 100 m within the ring (Figure 3). The only exception occurs between stations 4 and 5 because in this region the salinity is rather homogeneous in the uppermost 100 m. The surface velocities are only slightly smaller than the 100 m values. The total rotational mass transport is 33 Sv, with 28 Sv corresponding to the upper-thermocline AGW waters (from the sea surface to the 26.8 kg m^{-3} isoneutral) and 5 Sv representing the transport in the intermediate layers (isoneutral range from 26.8 to 27.75 kg m^{-3}).
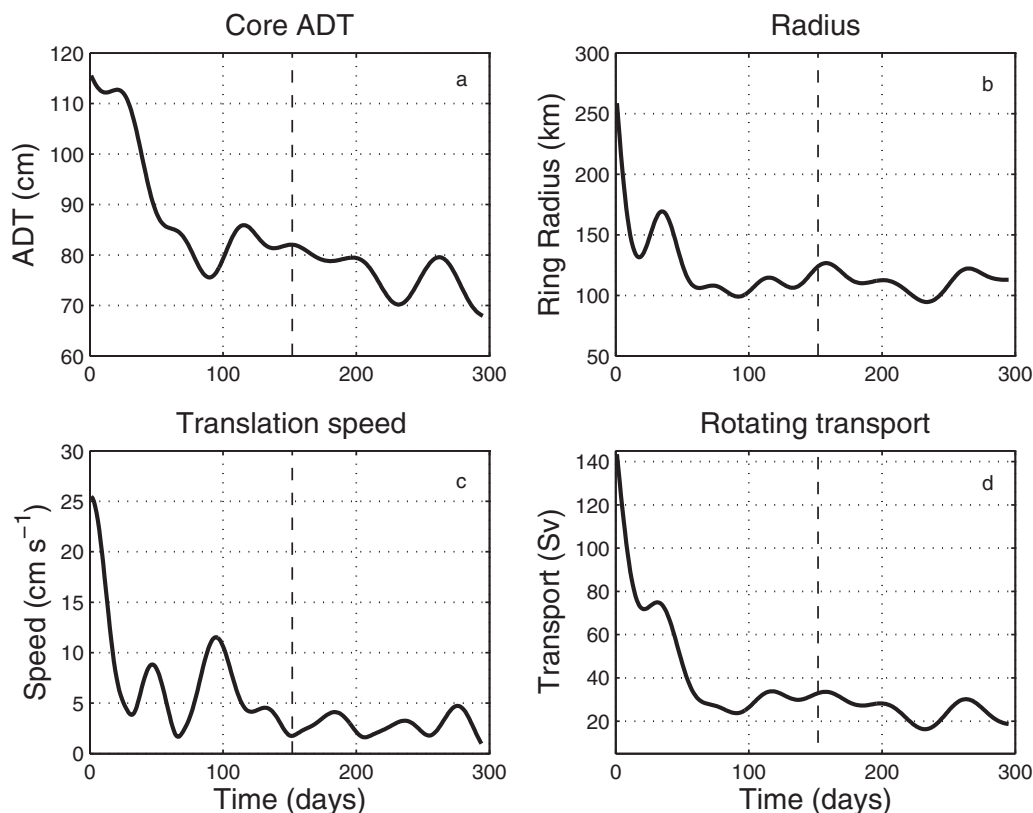
4. Temporal Ring Evolution

We complete our analysis investigating the short and long-term evolution of the ring. For the long-term changes, we employ the altimetry and hydrographic data, for the short-term evolution, we use the drifter data.

The long-term evolution of the ring's core ADT, radius, translation speed, and rotational transport is inferred from consecutive altimetry images (Figure 10) (the rotational transport is estimated using the simple method described in section 2.2). The ring ADT decayed significantly between October 2009 and March 2010 (days 1–150) at an average rate of 6.4 cm per month (Figure 10a); thereafter, the rate of ADT change slowed down to about 3 cm per month. The ring radius was about 260 km on 4 October 2010, just before the ring's shedding (Figure 10b) but decreased to some 125 km in just 1 month, shortly after completely detaching from the retroflection. From early December (day 60) till the end of the track, the ring radius oscillated between 94 and 127 km with a mean radius of about 110 km (124 km during the survey, on day 152).

During the first month, the time interval that the ring took to completely detach, the ring translated westward quite rapidly (Figures 5 and 10c). During the subsequent 2 months, the speed of translation oscillated markedly, in the range 2–12 cm s^{-1}, and later on it stabilized to about 3–4 cm s^{-1}. The ring rotation transport also had two phases (Figure 10d). During the first month the mass transport was quite large, in excess of 60 Sv, but by the end of the second month it had stabilized to values of 30–35 Sv, a situation that lasted for about 5 months. Only during the last couple of months the transport appeared to weaken again, occasionally decreasing to only 5 Sv.

The temporal evolution of all above quantities suggests a decay of the ring with time, likely through diffusion and mixing with the surrounding ocean. A variable that is adequate to estimate this rate decay is the relative vorticity, for solid-body type rotation it being equal to twice the angular velocity, $\zeta = 2\omega$. In a
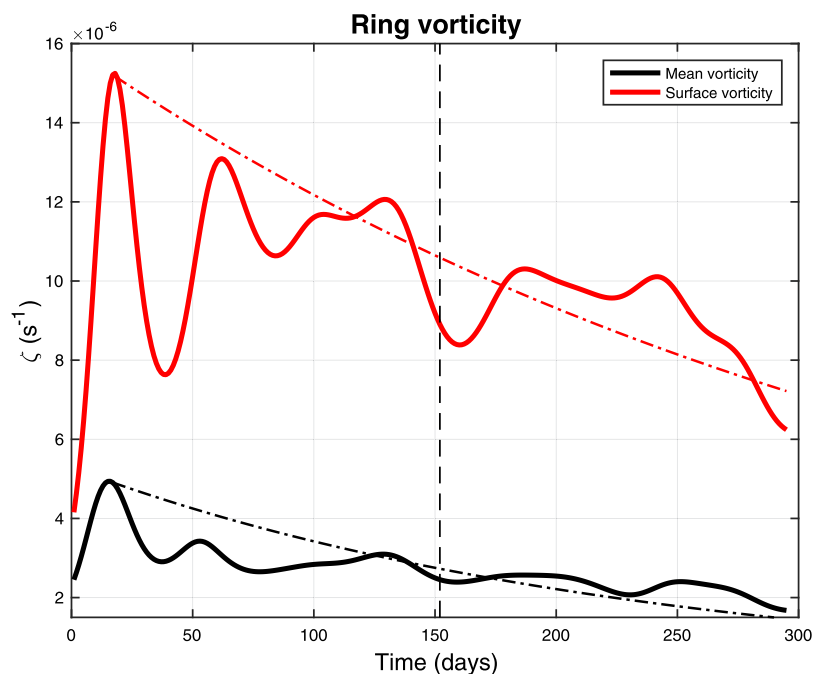
Figure 10. Temporal evolution of the ring parameters as obtained from the altimetry imagery, with the time running from 4 October 2009 (day 0) to 25 July 2010 (day 294): (a) core ADT (cm), (b) radius (km), (c) mean translation speed (cm s^{-1}), and (d) rotational transport (Sv). The dashed lines indicate 4 March 2010 (day 152), corresponding to the cruise survey.

nondivergent horizontal f-plane, a standard linear frictional term leads to an equation of the sort $d\zeta/dt = -\zeta/\tau$, where d/dt is the material derivative and τ is the temporal scale for decay. The solution of this equation is $\zeta(t) = \zeta_0 \exp(-t/\tau)$, where $\zeta_0 \equiv \zeta(t=0)$ is the initial relative vorticity. We may apply this expression to either the surface or the vertical-mean vorticity, as briefly described next.

The surface vorticity is calculated as twice the angular velocity, or twice the mean tangential velocity divided by half the radius R, with the mean tangential velocity (v) estimated (assuming geostrophic balance) from the ADT difference between the ring core and the 0.5 m contour ($\delta\eta$); hence, the surface vorticity is equal to $\zeta_s = 4v/R = 4g \ \delta\eta/(fR^2)$, where g is the gravity acceleration and f is the Coriolis parameter. Alternatively, the vertical-mean vorticity ζ_m of the ring may be estimated from its rotational transport, as if it was a cylinder of radius R and depth h. Assuming again solid-body rotation, the rotational transport may be estimated as $T = (h\omega R^2)/2$, so the mean vorticity becomes $\zeta_m = 2\omega = 4T/(hR^2)$.

The temporal evolution of the ring's surface and the vertical-mean vorticities is calculated using the above expressions (Figure 11). The best-fit exponential decay is calculated for either variable using the corresponding maximum vorticity values, set just after the complete shedding of the ring, as the initial value. The time scales calculated in this way are 230 days for the mean vorticity and 373 days for the surface vorticity.

We may also explore what would be the decay time scales for the temperature $\delta\theta$ and salinity δS anomalies brought to the subantarctic South Atlantic waters by the ring. For this purpose, we also use exponentially decaying expressions for both quantities, i.e., $\delta S(t) = \delta S_0 \exp(-t/\tau)$, where $\delta S_0 \equiv \delta S(t=0)$, and an analogous expression for θ. (note that the vorticity anomaly equals the vorticity itself because of near-zero background values.) The initial anomaly δS_0 is calculated as the difference between the value of the property at the core of the AC before retroflection and the salinity of the environmental eastern South Atlantic waters along 39°S (data comes from sections A13 in the South Atlantic Ocean and I06 in the Indian Ocean). The

Figure 11. Temporal evolution of the surface (red lines) and vertical-mean (black lines) vorticities of the ring (s^{-1}) as deduced from the altimetry data, with the time running from 4 October 2009 (day 0) to 25 July 2010 (day 294). The solid lines denote the values inferred from the observations and the dash-dotted lines represent the best-fit exponential decay, starting from the peak vorticity values shortly after generation. The vertical dashed line indicates 4 March 2010 (day 152), corresponding to the cruise survey.

anomaly on 4 March is calculated as the difference between the values at station 3 and the environmental eastern South Atlantic waters along 39°S. For our calculations, we have selected the 200 m water level, as it corresponds to the maximum salinity values at station 3, the ring core in the salinity vertical section (Figure 3b). The time scales calculated in this way are 276 days for salinity and 243 days for temperature, somewhere in between the two values obtained from the two vorticity time series (230 and 373 days).

We conclude looking at the information brought about by the drifters on the evolution of the radial structure of the ring. The ring stayed fairly stable while the drifters remained inside the ring, corresponding to days 152–205 (10 March to 18 April) of the altimetry time series (Figures 10 and 11). Therefore, we may use the radial position and period of revolution during this entire time interval in order to assess the radial distribution of the ring's surface vorticity. We compute the vorticity as $\zeta(r) = (4\pi)/T$, where the period is a function of the radial coordinate, $T = T(r)$, and draw the data points as a scattered plot (Figure 12a). The vorticity is fairly constant in a core region that goes from the ring's center to about 30–35 km, and decreases at larger radial positions. We may also plot the radial distribution of the tangential velocity, calculated as $v(r) = \omega r = (2\pi r)/T$ (Figure 12b). The tangential velocity increases almost linearly with the radial position until about 30–35 km, remaining fairly constant beyond.

The above vorticity and velocity data may be compared with the radial distribution expected for a Rankine vortex: (a) an inner region with a constant angular vorticity that decays in time, (b) a transition band with fairly constant tangential velocity that widens with time, and (c) an exterior region where the velocity decreases with radial distance [*Aboelkassem et al.*, 2005]. Indeed, our results suggest that the ring, during the period the drifters remained inside, behaved as viscous-decaying Rankine vortex, with the drifters moving between the inner region and the transition irrotational band.

Placing these results in the observed long-term trend (Figures 10a and 10b), the lowering in the core ADT brings about a decline in the rate of rotation of the inner core (at a rate that decreases with time) while the radius remained fairly constant during most of the lifetime of the ring (about 110 km) (Figure 10b). Remarkably, these results agree well with the solution by *Aboelkassem et al.* [2005], which predicts the same sort of variations for the angular velocity and size of the inner core.
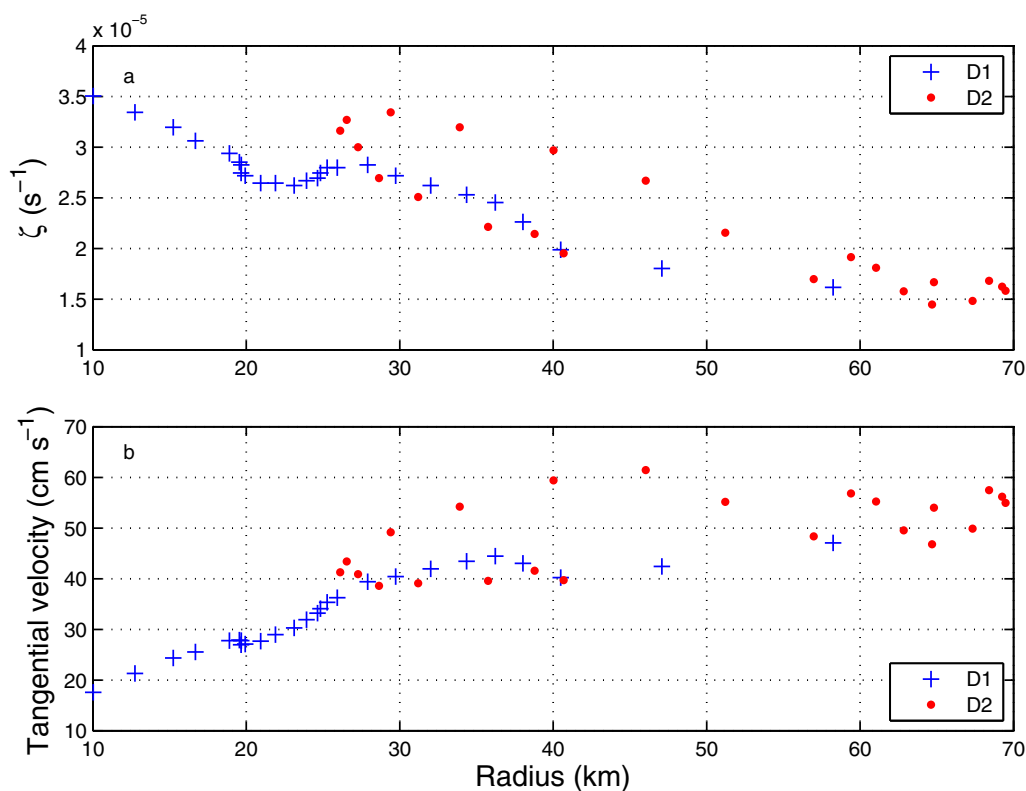
Figure 12. Daily mean (a) surface vorticity (s^{-1}) and (b) tangential velocity (cm s^{-1}) of the ring as deduced from drifters D1 (crosses) and D2 (dots). The data correspond to the time period from 10 March to 18 April 2010.

5. Discussion and Concluding Remarks

Hydrographic sampling along 39°S between 5 and 9°E, during the MOC2-Austral cruise on 4–5 March 2010, identified an anticyclonic structure enclosing water masses originated at the Agulhas Current (AC). This was an Agulhas ring, as also shown by daily ADT images that tracked its origin back to the AC retroflection (ACR). The ring was spawned in October 2009 with a maximum ADT of 1.15 m at the beginning of its life time (when it had not yet totally separated from the retroflection) that decreased to 0.83 m after 5 months (when surveyed). The surface signature of the ring disappeared on 25 July 2010 after fusing with other mesoscale structures. Therefore, according to *van Aken et al.* [2003], it can be classified as a strong Agulhas ring. The relatively fast decay of the ring's ADT during the first 152 days (about 5 cm per month) coincides with its crossing of the Benguela Current [*Drijfhout et al.*, 2003]. After this period, the core ADT decreased at a slower pace, about 3 cm per month, but still much faster than values (0.5 cm per month) previously reported by *Drijfhout et al.* [2003].

The CTD data during the MOC2-Austral cruise, carried out 5 months after the ring's shedding, show that the ring's hydrographic signature extended down to about the upper limit of the NADW (about 2000 m or $\gamma_n = 27.8$ kg m^{-3}) (Figure 4). The ring's hydrographic properties are a reflection of its baroclinic parent, the AC [*Garzoli et al.*, 1999], differing from those of the surrounding waters at the surface, subsurface, and intermediate waters. Water trapped inside the ring comes from the Indian Ocean: AGW at surface and subsurface surrounded by SAMW, and traces of RSW at the lower-intermediate waters enclosed by UCDW. In the upper-intermediate waters, between the SAMW-AGW and UCDW-RSW strata, we find fairly similar AAIW of Indian (Atlantic) origin inside (outside) the ring. The observed ring's water masses are similar to those found in other Agulhas rings [*McDonagh et al.*, 1999]; according to *Garzoli et al.* [1999], the appearance of RSW is intermittent.

The ring caused substantial perturbations in the salinity and temperature (and hence, density) structure down to about 2000 m, reflecting the presence of distinct source water types from the Indian Ocean. Between 2000 and 4500 m, there are no intruding water masses (Figure 4) but the isopycnals remained

slightly perturbed, as shown by the fact that the geostrophic velocity changed with depth until about 4500 m (Figure 9). Choosing the reference level at 4500 m, the maximum relative geostrophic velocities are found at about 100 m. The velocity decreased in depth to values less than 5 cm s^{-1} below 2000 m, marking the vertical extension of the ring. The maximum geostrophic velocities at the surface of the ring (about 30 cm s^{-1}) are comparable to those estimated by *Garzoli et al.* [1999] and *Duncombe Rae et al.* [1996], and lower than those obtained by *van Aken et al.* [2003] and *Olson and Evans* [1986], whom estimated velocities of about 1 m s^{-1} at the surface of the ring.

The geostrophic velocities lead to a counterclockwise rotational transport of 33 Sv, corresponding to 28 Sv in the surface and thermocline layers and 5 Sv at intermediate levels. Combining the CTD observations with the altimetry data has allowed us to obtain a time series of the rotational transport, which decreases from 140 Sv immediately after the ring's shedding to a fairly constant value of 30–35 Sv until month 10, before merging with other mesoscalar features. These transports are similar to values reported by *Gordon and Haxby* [1990], in the range of 20–30 Sv within the upper 1500 m of the water column.

A more detailed description of the ring's surface circulation is obtained from the trajectories of two drifters (D1 and D2) deployed during the cruise: these drifters lasted about 50 days inside the ring, from early March until mid-April or months 6–7 after shedding. The rotational period is obtained from both wavelet analysis and the drifter trajectories decomposition, showing very consistent results (Figures 7 and 8). D1 was deployed in the ring's core and remained there for about 30 days, rotating with a period of 4–6 days, before moving to the ring's outer band where the period was substantially longer (about 10 days). D2 behaved different, being initially in the outer part of the ring and moving to the inner core between about days 180 and 190, at about the same time as D1 moved out; however, D2 did not remain there very long as shortly after it left the ring. The rotational period of the inner core is substantially shorter than reported by *Richardson* [2007], who found a ring rotating with a 10-day period southeast of Cape Basin (after formation) and increasing to 20–40 days as it moved west.

Since the ring did not change substantially during the time the drifters remained inside (Figures 2 and 10), we have used all the drifters' periods and orbital velocities to plot both the surface vorticity and orbital velocity as a function of radial coordinate. The results strongly suggest that the ring behaved as a decaying Rankine vortex, with an inner core in solid-body type rotation with angular velocity that remained fairly constant with time and a transition band characterized by near-constant tangential velocities [*Aboelkassem et al.*, 2005; *Sangrà et al.*, 2005]; further away from the center, there is possibly another region where the velocity decays with radial distance [*Aboelkassem et al.*, 2005]. The time intervals spent by both drifters in these different regions, and the large oscillations they displayed as they left the core, suggest that the inner core is very stable but both the transition band and particularly the exterior region experience large radial perturbations.

According to the ADT imagery and the drifters' trajectories, the ring moved northwest along the Agulhas Ring Corridor [*Garzoli and Gordon*, 1996], through the southern route followed by ∼23% of the rings [*Dencausse et al.*, 2010]. Similarly as it happened with the core ADT decay, the ring's translation speed and radius may be decomposed in two phases (Figure 10). The first one lasted while the ring crossed the Benguela Current system, with a relatively large radius (150 km or larger) and substantial changes in mean speed (2–25 cm s^{-1}), possibly still feeling the impulse experienced during its shedding from the AC. During the second phase, once completely separated from the ACR, the ring had a more constant mean velocity, of about 4 cm s^{-1} (from both D1 and altimetry) or 7 cm s^{-1} (from D2), and its radius remained fairly constant at about 110 km. *Garzoli et al.* [1999] and *Gordon and Haxby* [1990] using altimetry data found rings with radius in the range of 100–150 km.

The mean northward velocity component for the ring may be estimated either from altimetry or from the drifters. Altimetry between day 30 (when the ring was located near 40.2°S) and the end of the time series grants a mean northward velocity of 1.2 cm s^{-1}; the values estimated from the drifters are slightly larger, about 1.5 and 1.9 cm s^{-1}, respectively, for D1 and D2. Using a mean speed of 1.2 cm s^{-1} and the heat contained within the eddy lends a heat transport of 0.2 PW, which would be a significant contribution to the total 0.7 PW that cross the A11 section [*Ganachaud and Wunsch*, 2000]. Nevertheless, the relevance of this value depends on whether the ring, maintained as a unity, could enter the tropical gyre. The answer is that it neither remains as an entity nor crosses beyond 20°S [*Lutjeharms*, 2007]. Hence, the key issue is on how the ring's content of heat and other properties is incorporated into the subtropical gyre.

To address this point, we have assessed the ring's decay within the South Atlantic, as deduced from its vorticity, temperature, and salinity. Fitting the results to an exponential function, we find a decay time-scale of the order of 1 year. This confirms that most of the property anomalies contained within the ring will be transferred to the South Atlantic subtropical gyre before the ring reaches the American continent, so that their meridional transfer will take place at the rate of the subtropical-tropical exchange. Hence, we are left to examine whether the rings provide a significant contribution to the mean property values in the surface and intermediate layers of the South Atlantic, the layers that represent the returning limb of the AMOC.

The answer to this last question is related to the product of the ring's property anomaly and fractional volume or, since the rings reach down to the intermediate layers, the property anomaly in the thermocline and intermediate layers times the surface fraction the rings occupy in the Agulhas Ring Corridor, i.e., the region that effectively contributes to the subtropical-tropical transfer [*Lazar et al.*, 2002; *van Sebille et al.*, 2012; *Blanke et al.*, 2015]. This region is a relatively narrow band between the subtropical and tropical oceans, roughly 5° wide and running between 15°E and 40°W. Considering that every year (the ring's decay time) about six rings find their way along the Agulhas Ring Corridor, and that each of these rings occupies an initial radius of 150 km, their fractional area (area of the rings divided by the area of the Corridor) is about 0.15. Given a property anomaly Δ over a background value of C, then the environment water will contribute 0.85C and the rings will account for 0.15(C+Δ), or a fractional contribution of 15Δ/100C. For heat, C$\cong$16°C and $\Delta\cong$5° (near the sea surface) so the fractional contribution will reach no more than 5%; repeating the argument for salinity leads to even smaller values.

We may conclude that, despite their regional relevance, the Agulhas rings do not contribute substantially to the latitudinal heat and salt transport by the returning limb of the AMOC. Therefore, most of the change in latitudinal heat transport between 35 and 19°S, from 0.35 and 0.77 PW according to *Ganachaud and Wunsch* [2003], must be the result of heat incorporated through the warming of the subantarctic waters as they recirculate within the subtropical South Atlantic.

References

Aboelkassem, Y., G.H. Vatistas, and N. Esmail (2005), Viscous dissipation of Rankine vortex profile in zero meridional flow, *Acta Mech. Sin.*, 21, 550–556, doi:10.1007/s10409-005-0073-3.

Arhan, M., H. Mercier, and J. R. E. Lutjeharms (1999), The disparate evolution of three Agulhas rings in the South Atlantic Ocean, *J. Geophys. Res.*, 104(C9), 20,987—21,005, doi:10.1029/1998JC900047.

AVISO (2015), SSALTO/DUACS User Handbook: (M)SLA and (M)ADT Near-Real Time and Delayed Time Products, CLS, 4.4th ed., sALP-MU-P-EA21065-CLS, Toulouse, France.

Barré, N., C. Provost, C. Renault, and N. Sennéchael (2011), Fronts, meanders and eddies in Drake Passage during the ANT-XXIII/3 cruise in January-February 2006: A satellite perspective, *Deep Sea Res., Part II*, 58, 2533–2554, doi:10.1016/j.dsr2.2011.01.003.

Biastoch, A., and W. Krauss (1999), The role of mesoscale eddies in the source regions of the Agulhas current, *J. Phys. Oceanogr.*, 29, 2303–2317.

Biastoch, A., C.W. Böning, and J. R. E. Lutjeharms (2008), Agulhas leakage dynamics affects decadal variability in Atlantic overturning circulation, *Nature*, 456, 489–492, doi:10.1038/nature07426.

Blanke, B., S. Speich, and E. Rusciano (2015), Lagrangian water mass tracing from pseudo-Argo, model-derived salinity, tracer and velocity data: An application to Antarctic Intermediate Water in the South Atlantic Ocean, *Ocean Modell.*, 85, 56–67, doi:10.1016/j.ocemod.2014.11.004.

Brassington, G. B. (2010), Estimating surface divergence of ocean eddies using observed trajectories from a surface drifting buoy, *J. Atmos. Oceanic Technol.*, 27, 705–720, doi:10.1175/2009JTECHO651.1.

Dencausse, G., M. Arhan, and S. Speich (2010), Routes of Agulhas rings in the southeastern Cape Basin, *Deep Sea Res., Part I*, 57, 1406–1421, doi:10.1016/j.dsr.2010.07.008.

Drijfhout, S. S., C. A. Katsman, L. de Steur, P. C. F. van der Vaart, P. J. van Leeuwen, and C. Veth (2003), Modeling the initial, fast sea-surface height decay of Agulhas ring "Astrid," *Deep Sea Res., Part II*, 50, 299–319, doi:10.1016/S0967-0645(02)00386-7.

Duncombe Rae, C. M., S. L. Garzoli, and A. L. Gordon (1996), The eddy field of the southeast Atlantic Ocean: A statistical census from the Benguela sources and transports project, *J. Geophys. Res.*, 101(C5), 11,949–11,964, doi:10.1029/95JC03360.

Ganachaud, A. (2003), Large-scale mass transports, water mass formation, and diffusivities estimated from World Ocean Circulation Experiment (WOCE) hydrographic data, *J. Geophys. Res.*, 108(C7), 3213, doi:10.1029/2002JC001565.

Ganachaud, A., and C. Wunsch (2000), Improved estimates of global ocean circulation, heat transport and mixing from hydrographic data, *Nature*, 408, 453–457, doi:10.1038/35044048.

Ganachaud, A., and C. Wunsch (2003), Large-scale ocean heat and freshwater transports during the World Ocean Circulation Experiment, *J. Clim.*, 16, 696–705.

Garzoli, S. L., and A. L. Gordon (1996), Origins and variability of the Benguela Current, *J. Geophys. Res.*, 101(C1), 897–906, doi:10.1029/95JC03221.

Garzoli, S. L., P. L. Richardson, C. M. Duncombe Rae, D. M. Fratantoni, G. J. Goñi, and A. J. Roubicek (1999), Three Agulhas rings observed during the Benguela Current Experiment, *J. Geophys. Res.*, 104(C9), 20,971–20,985, doi:10.1029/1999JC9000605.

González-Dávila, M., J. M. Santana-Casaiano, R. A. Fine, J. Happell, B. Delille, and S. Speich (2011), Carbonate system in the water masses of the Southeast Atlantic sector of the Southern Ocean during February and March 2008, *Biogeosciencies*, 8, 1401–1413, doi:10.5194/bg-8-1401-2011.

Gordon, A. L., and W. F. Haxby (1990), Agulhas eddies invade the south Atlantic: Evidence from Geosat altimeter and shipboard conductivity-temperature-depth survey, *J. Geophys. Res.*, *95*(C3), 3117–3125, doi:10.1029/JC095iC03p03117.

Gordon, A. L., R. F. Weiss, W. M. Smethie Jr., and M. J. Warner (1992), Thermocline and intermediate water communication between the south Atlantic and Indian Oceans, *J. Geophys. Res.*, *97*(C5), 7223–7240, doi:10.1029/92JC00485.

Hernández-Guerra, A., J. L. Pelegrí, E. Fraile-Nuez, V. Benítez-Barrios, M. Emelianov, M. D. Pérez-Hernández, and P. Vélez-Belchí (2014), Meridional overturning transports at 7.5N and 24.5N in the Atlantic Ocean during 1992–93 and 2010–11, *Prog. Oceanogr.*, *128*, 98–114, doi:10.1016/j.pocean.2014.08.016.

Lazar, A., T. Inui, P. Malanotte-Rizzoli, A. J. Busalacchi, L. Wang, and R. Murtugudde (2002), Seasonality of the ventilation of the tropical Atlantic thermocline in an ocean general circulation model, *J. Geophys. Res.*, *107*(C8), 3104, doi:10.1029/2000JC000667.

Lumpkin, R, S. A. Grodsky, L. Centurioni, M.-H. Rio, J. A. Carton, and D. Lee (2013), Removing spurious low-frequency variability in drifter velocities, *J. Atmos. Oceanic Technol.*, *30*, 353–360, doi:10.1175/JTECH-D-12-00139.1.

Lutjeharms, J. R. E. (2007), Three decades of research on the greater Agulhas Current, *Ocean Sci.*, *3*, 129–147.

Lutjeharms, J. R. E., and I. J. Ansorge (2001), The Agulhas return current, *J. Mar. Syst.*, *30*, 115–138, doi:10.1016/S0924-7963(01)00041-0.

Mason, E., A. Pascual, P. Gaube, S. Ruiz, J. L. Pelegrrí, and A. Delepoulle (2017), Subregional characterization of mesoscale eddies across the Brazil-Malvinas Confluence, *J. Geophys. Res. Oceans*, *122*, 3329–3357, doi:10.1002/2016JC012611.

McDonagh, E. L., K. J. Heywood, and M. P. Meredith (1999), On the structure, paths, and fluxes associated with Agulhas rings, *J. Geophys. Res.*, *104*(C9), 21,007–21,020, doi:10.1029/1998JC900131.

Mercier, H., et al. (2015), Variability of the meridional overturning circulation at the Greenland-Portugal OVIDE section from 1993 to 2010, *Prog. Oceanogr.*, *132*, 250–261, doi:10.1016/j.pocean.2013.11.001.

Olson, D. B., and R. H. Evans (1986), Rings of the Agulhas current, *Deep Sea Res., Part A*, *33*, 27–42, doi:10.1016/0198-0149(86)90106-8.

Orsi, A. H., T. Whitworth III, and W. D. Nowlin Jr. (1995), On the meridional extent and fronts of the Antarctic Circumpolar Currents, *Deep Sea Res., Part I*, *42*, 641–673, doi:10.1016/0967-0637(95)00021-W.

Rahmstorf, S., and M. H. England, (1997), Influence of Southern Hemisphere winds on North Atlantic Deep Water flow, *J. Phys. Oceanogr.*, *27*, 2040–2054.

Richardson, P. L. (2007), Agulhas leakage into the Atlantic estimated with subsurface floats and surface drifters, *Deep Sea Res., Part I*, *54*, 1361–1389, doi:10.1016/j.dsr.2007.04.010.

Richardson, P. L., J. R. E. Lutjeharms, and O. Boebel (2003), Introduction to the "Inter-ocean exchange around southern Africa," *Deep Sea Res., Part II*, *50*, 1–12, doi:10.1016/S0967-0645(02)00376-4.

Rodrigues, R. R., L. M. Rosthstein, and M. Wimbush (2007), Seasonal variability of the South Equatorial current bifurcation in the Atlantic Ocean: A numerical study, *J. Phys. Oceanogr.*, *37*, 16–30, doi:10.1175/JPO2983.1.

Sangrà, P., J. L. Pelegrí, A. Hernández-Guerra, I. Arregui, J. M. Martín, A. Marrero-Díaz, A. Martínez, A, W. Ratsimandresy, and A. Rodríguez-Santana (2005), Life history of an anticyclonic eddy, *J. Geophys. Res.*, *110*, C03021, doi:10.1029/2004JC002526.

Schouten, M. W., W. P. M. de Ruijter, and P. J. van Leeuwen (2000), Translation, decay and splitting of Agulhas rings in the Southeastern Atlantic Ocean, *J. Geophys. Res.*, *105*(C9), 21,913–21,925, doi:10.1029/1999JC000046.

Souza, J. M. A. C., C. de Boyer Montégut, C. Cabanes, and P. Klein (2011), Estimation of the Agulhas ring impacts on meridional heat fluxes and transport using ARGO floats and satellite data, *Geophys. Res. Lett.*, *38*, L21602, doi:10.1029/2011GL049359.

Toggweiler, J. R., and B. Samuels (1995), Effect of Drake Passage on the global thermohaline circulation, *Deep Sea. Res., Part I*, *42*, 477–500, doi:10.1016/0967-0637(95)00012-U.

Torrence, C., and G. P. Compo (1998), A practical guide to wavelet analysis, *Bull. Am. Meteorol. Soc.*, *79*, 61–78.

Tsuchiya, M., L. D. Talley, and M. S. McCartney (1994), Water-mass distribution in the western South Atlantic; A section from South Georgia Island (54S) northward across the equator, *J. Mar. Res.*, *52*, 55–81, doi:10.1357/0022240943076759.

van Aken, H. M., A. K. van Veldhoven, C. Veth, W. P. M. de Ruijter, P. J. van Leeuwen, S. S. Drijfhout, C. P. Whittle, and M. Rouault (2003), Observations of a young Agulhas ring, Astrid, during MARE in March 2000, *Deep Sea Res., Part II*, *50*, 167–195, doi:10.1016/S0967-0645(02)00383-1.

van Sebille, E., W. E. Johns, and L. M. Beal (2012), Does the vorticity flux from Agulhas rings control the zonal pathway of NADW across the South Atlantic?, *J. Geophys. Res.*, *117*, C05037, doi:10.1029/2011JC007684.

Wang, Y., M. J. Olascoaga, and F. J. Beron-Vera (2015), Coherent water transport across the South Atlantic, *Geophys. Res. Lett.*, *42*, 4072–4079, doi:10.1002/2015GL064089.

Wang, Y., F. J. Beron-Vera, and M. J. Olascoaga (2016), The life cycle of a coherent Lagrangian Agulhas ring, *J. Geophys. Res. Oceans*, *121*, 3944–3954, doi:10.1002/2015JC011620.